PCCP

RSC Publishing

PAPER

View Article Online
View Journal

Cite this: DOI: 10.1039/c3cp51937f

Hydration water and peptide dynamics – two sides of a coin. A neutron scattering and adiabatic calorimetry study at low hydration and cryogenic temperatures

Margarida Bastos,*[a] Nuno Alves,[a] Sílvia Maia,[a] Paula Gomes,[a] Akira Inaba,[b] Yuji Miyazaki[b] and Jean-Marc Zanotti*[c]

Received 15th May 2013,
Accepted 12th July 2013

DOI: 10.1039/c3cp51937f

www.rsc.org/pccp

In the present work we bridge neutron scattering and calorimetry in the study of a low-hydration sample of a 15-residue hybrid peptide from cecropin and mellitin CA(1–7)M(2–9) of proven antimicrobial activity. Quasielastic and low-frequency inelastic neutron spectra were measured at defined hydration levels – a nominally 'dry' sample (specific residual hydration h = 0.060 g/g), a H_2O-hydrated (h = 0.49) and a D_2O-hydrated one (h = 0.51). Averaged mean square proton mobilities were derived over a large temperature range (50–300 K) and the vibrational density of states (VDOS) were evaluated for the hydrated samples. The heat capacity of the H_2O-hydrated CA(1–7)M(2–9) peptide was measured by adiabatic calorimetry in the temperature range 5–300 K, for different hydration levels. The glass transition and water crystallization temperatures were derived in each case. The existence of different types of water was inferred and their amounts calculated. The heat capacities as obtained from direct calorimetric measurements were compared to the values derived from the neutron spectroscopy by way of integrating appropriately normalized VDOS functions. While there is remarkable agreement with respect to both temperature dependence and glass transition temperatures, the results also show that the VDOS derived part represents only a fraction of the total heat capacity obtained from calorimetry. Finally our results indicate that both hydration water and the peptide are involved in the experimentally observed transitions.

1. Introduction

It is widely accepted that water plays a fundamental role in biological systems. Nevertheless, many aspects regarding its particular structure near the surface and inside biological macromolecules as well as its link to biological function are still under discussion.[1–17] Proteins are known to have a "limiting hydration" necessary for function, and thus there must exist a link between hydration and protein functional properties.

Since Sturtevant's seminal paper[18] on the sources of heat capacity and entropy changes in proteins, the molecular dynamics of many processes involving proteins and peptides have become amenable to detailed study by experimental techniques and also by simulation. Neutron scattering techniques are highly informative here because of the close Fourier-transform relation of neutron spectra to basic space–time correlation functions obtained from molecular dynamics (MD) simulations.[19]

Biophysical studies using energy-resolving neutron techniques have largely been concerned with the evolution of the 'energy landscape' of slightly D_2O-hydrated biomolecules by way of measuring $\langle u^2 \rangle$ as a function of temperature T between $\sim$30 and 300 K.[20–24] Thus studies are available on water at or near biomolecular surfaces,[1,2,9,12,14,16,17,25–29] the coupling between the hydration shell and interior modes,[14] and the effect of cosolvents,[5] and complementing ^{1}H NMR (Nuclear Magnetic Resonance) and MD simulations, in the study of the mechanisms of biopolymer–water interactions in hydrated powders, peptides, proteins, and DNA fibers (see *e.g.* ref. 1, 2, 5, 14, 17, 20 and 30–33).

Calorimetry has been widely used to study biomacromolecules, like proteins, enzymes or DNA. Most studies are performed in solution, mostly by Differential Scanning Calorimetry (DSC) or Isothermal Titration Calorimetry (ITC). DSC encompasses stability studies, providing the thermodynamic parameters characterizing the denaturation process – T_m, ΔH_m(cal) and ΔH_m(van't Hoff) and ΔC_p are extracted.[3,4,10,34–37] ITC is used in ligand-binding experiments and the thermodynamic parameters for the interaction are derived (K and ΔH, and if experiments are made at different temperatures also ΔC_p).[6,38–45] To a much smaller extent, calorimetric

[a] CIQ (UP), Department of Chemistry and Biochemistry, Faculty of Sciences, University of Porto, R. Campo Alegre 687, P-4169-007 Porto, Portugal. E-mail: mbastos@fc.up.pt; Fax: +351 22 0402659
[b] Research Center for Structural Thermodynamics, Graduate School of Science, Osaka University, Toyonaka, Osaka 560-0043, Japan
[c] LLB (CEA-CNRS), CEA Saclay, 91191 Gif/Yvette cedex, France. E-mail: jean-marc.zanotti@cea.fr; Fax: +33 1 69088261

measurements on proteins or DNA at low hydration have also been performed.[7,8,46–48] The water molecules that make up the hydration shell in the immediate vicinity of the surface of a protein or DNA are particularly relevant to their function, as well as in protein–DNA interactions. Therefore, this type of determination provides extremely useful information. One of the reasons for the scarce amount of experimental heat capacity data down to very low temperatures is the very limited number of high sensitivity low-temperature adiabatic calorimeters around the world that can handle small amounts of sample with low conductivity (such as the biomacromolecules), in contrast to common samples in material science studies using low-temperature calorimetry.

Attempts to bridge results from different techniques are not abundant, and yet are fundamental for a full understanding of the studied phenomena since different techniques sample different time and space scales. Previously, some of us conducted a study where neutron scattering and earlier calorimetric results were compared so as to ascertain the amount and dynamics of "unfreezable water".[1,7,8] Zanotti *et al.*[14] have studied the hydration coupled dynamics in parvalbumin by combining QENS/INS and NMR, and more recently they addressed the problem of the existence of a liquid–liquid transition of water on Vycor samples by a combination of calorimetric (DSC) and diffraction data.[49] Lerbret *et al.*[50] performed a Raman scattering and MD simulation study of the low-frequency vibrational properties of lysozyme in sugar aqueous solutions, and Russo *et al.*[51] compared inelastic neutron scattering and molecular dynamics simulations to investigate low-frequency modes of hydration water in selected hydrophilic and hydrophobic biomolecules. Recently Jansson and Swenson[52] did characterize the myoglobin glass transition in water and water–glycerol mixtures by dielectric spectroscopy and DSC.

The potential of inelastic neutron scattering for deducing thermodynamic properties of biopolymers by way of integrating low-frequency spectra and extracting their vibrational density of states (VDOS) was recognized more than 40 years ago.[53] Boutin and Whittemore[54] measured neutron spectra for polycrystalline samples of polyglutamic acid in the 30 to 600 cm^{-1} region and derived approximate values for the thermodynamic quantities characterizing the helix to random-coil transition which agreed reasonably well with other data. Nevertheless, very few attempts have been made to quantify the vibrational density of states (VDOS) of biomolecules with the aim of understanding their calorimetric and kinetic properties at the molecular level.

The present work contributes to this bridging effort, presenting and discussing results from a first combined neutron scattering and calorimetric study of the low-temperature dynamics of an antimicrobial oligopeptide. Antimicrobial peptides (AMPs) are a promising new antibiotics paradigm. One particularly successful approach is based on hybrid sequences derived from naturally occurring α-helical AMPs, of which cecropin A (CA) and melittin (M) provided the first examples of AMP sequence hybridization. The hybrids share the cationic N-terminus of cecropin A followed by the hydrophobic N-terminus of melittin. One particularly successful member of this family is CA(1–7)M(2–9), which we have been studying by a variety of biophysical methods.[55,56] The peptide has a random structure in aqueous solution, and acquires an α-helix secondary structure in the presence of membranes.

Thus (i) the temperature dependence of proton mobilities (averaged mean square proton mobilities), $\langle u^2 \rangle$, of three peptide samples were calculated – a nominally dry peptide (residual specific hydration h = 0.060 g/g), an H_2O-hydrated one (h = 0.49) and a D_2O-hydrated one (h = 0.51); and (ii) the trends of C_p values calculated from the neutron derived VDOS functions for both H_2O and D_2O hydrated samples were compared with the heat capacity (C_p) data obtained by adiabatic low temperature heat capacity calorimetry, in a large temperature range. The isotopic effect used here in INS/QENS is a unique way to disentangle the contributions of the hydration water and of the polypeptide itself to the C_p as measured by adiabatic calorimetry. It should nevertheless be noted that the times-scale probes by QENS and calorimetry are different. While calorimetry integrates the contributions of all the dynamical modes up to hundreds of seconds, it should be noted that in inelastic neutron scattering, this integration is performed on a much shorter time-scale. The cut-off at long times is controlled by the energy resolution of the spectrometer. In our case, the integration is performed up to few tens of ps.

2. Experimental section

2.1. Peptide synthesis

CA(1–7)M(2–9) is a hybrid peptide comprising the first 7 amino acid residues from cecropin A and the first 8 from melittin with sequence H-KWKLFKK-IGAVLKVL-NH_2. A large sample of the peptide (350 mg) was synthesized as a C-terminal carboxamide by Fmoc/*t*Bu solid phase strategies, and purified and characterized by methods as those described in Gomes *et al.*[57] Fmoc-protected amino acids, coupling reagents and resins for solid-phase peptide synthesis were purchased from Nova Biochem (Switzerland). All other reagents were from Sigma-Aldrich Co. LLC (St Louis, MO).

2.2. Sample preparation

2.2.1. For neutron scattering experiments. The residual, structurally essential water content of the nominally dry sample was h = 0.060 (g H_2O/g CA(1–7)M(2–9)) as measured by coulometry (Karl Fischer coulometer, 737 KF Metrohm). A total of 137 mg of this sample was spread out over a flat rectangular aluminum cell (22 × 35 mm) and tightly sealed. A peptide sample from the same batch was thereafter H_2O-hydrated by exposing it to a high relative humidity (RH) atmosphere, over a saturated solution of K_2SO_4 in H_2O at 5 °C (RH 98.5% at 5 °C). It was weighed daily, until it reached a specific hydration of h = 0.49 (which includes the h = 0.060 residual water content of the nominally dry sample). This sample, of total weight 548 mg, was loaded into an identical aluminum cell and sealed in the same way. A D_2O-hydrated C7M9 sample was prepared by dissolving the previous sample in D_2O and lyophilizing it. This was repeated twice, followed by KF titration to determine the final D_2O content. The coulometrically obtained value was corrected by the ratio of molecular weights of H_2O and D_2O [m (D_2O) = m (read in KF) × 20.03/18.02], resulting in h = 0.18 (g D_2O/g CA(1–7)M(2–9))

Table 1 Incoherent and coherent scattering cross-sections σ_{inc} and σ_{coh} for CA(1–7)M(2–9) hydrated with H_2O (h = 0.49) and D_2O (h = 0.51) forms. The values of the fractional scattering contributions relative to σ_{total} can be seen between brackets

	Peptide		H_2O		
H_2O hydrated	H	D	D	H	Total
σ_{coh} [a]	265.76 (1.2%)	—	—	169.13 (0.8%)	1430.96 (6.7%)
σ_{inc} [a]	12 120.77 (56.9%)			7713.45 (36.2%)	19 884.72 (93.3%)
$\sigma_{total} = \sigma_{inc} + \sigma_{coh}$					21 315.7
	Peptide		D_2O		
D_2O hydrated	H	D	D	H	Total
σ_{coh} [a]	207.68 (1.8%)	184.47 (1.6%)	505.93 (4.4%)	—	1882.35 (16.2%)
σ_{inc} [a]	9471.86 (81.5%)	67.65 (0.6%)	185.54 (1.6%)		9735.55 (83.8%)
$\sigma_{total} = \sigma_{inc} + \sigma_{coh}$					11 617.9

[a] σ_{inc}, σ_{coh} and σ_{total} in barn (10^{-24} cm^2).

for the D_2O-exchanged nominally dry sample. In a procedure similar to that used for H_2O hydration, this sample was then rehydrated over D_2O up to a level of h = 0.51, determined by weighing. A total of 324 mg of this sample was loaded into a cell and sealed as described above.

Peptides scatter neutrons coherently as well as incoherently, and both components yield structural and dynamical information in the form of dynamic structure factors $S_{coh}(Q,\omega)$ and $S_{inc}(Q,\omega)$ which relate closely to fundamental space–time correlation functions.[58] The large proton incoherent scattering dominates by a factor of $\sim$10 over all other contributions even after D_2O exchange and low-level D_2O hydration. The datasets obtained thus represent $S_{inc}(Q,\omega)$ functions which form the basis for analysis in terms of $g(\omega)$ and $\langle u^2\rangle$. Table 1 shows the calculated total neutron scattering cross-sections σ_{inc} and σ_{coh} for the H_2O and D_2O hydrated samples in order to provide a rough idea of the relative scattering powers expected for the sample conditions used.

2.2.2. For adiabatic calorimetry. From the hydrogenous, nominally dry sample, with an initial water content of h = 0.060 as above, a fully hydrated sample with h = 4.51 (g H_2O/g CA(1–7)M(2–9)) was prepared by adding degassed milli-Q water and keeping it at room temperature for about one week to attain equilibrium. From this sample, the h = 0.49 and h = 0.14 samples were obtained by drying in a dry helium atmosphere. Each sample was kept thereafter at room temperature for several days, prior to the heat capacity determination. The water contents of the hydrated samples were calculated from the mass difference relative to the nominally dry sample.

2.3. Neutron scattering experiments

2.3.1. Data collection. Neutron scattering experiments were performed at Laboratoire Léon Brillouin (Saclay, France) using a time-of-flight (TOF) spectrometer (MIBEMOL).

In order to maximize the flux on the sample, MIBEMOL has been used in a low resolution mode, with an incident wavelength of 5 Å, resulting in a triangular resolution function with full width at half maximum (FWHM) or R = 195 μeV at ω = 0. The flat rectangular cell was placed at an angle of 42.5° (hydrated sample) and 48.8° (dry sample) to the incident neutron beam and the scattered neutrons were detected at angles from 23.5° to 141.8°, corresponding to a range of accessible values of the elastic momentum exchange.

For the H_2O hydrated sample, two types of measurements were performed: (a) pure inelastic measurement: sampling times of 6–10 hours were used at 8 temperature points between 99 and 271 K; (b) the so-called elastic scan: a continuous 8-hour scan during which spectra were taken every 7 minutes. For the nominally dry sample we performed experiments with sampling times of 1–4 hours each, at about the same temperatures as those used for the long runs of the hydrated sample. For the D_2O hydrated sample, sampling times of 8–11 hours were used at 24 temperature points between 50 and 290 K.

The detector efficiency was determined by running the spectra of a vanadium sample having the same geometry of the sample. The spectrum of the empty container was also recorded, and used to correct all experiments.

2.3.2. Data analysis. QENSH,[59] the standard data analysis software of MIBEMOL, was used to correct the data, to normalise them with respect to monitor counts and vanadium run and to analyse them as described below. Neither multiple-scattering nor multi-phonon corrections were applied since their effect on integral properties of the spectra was considered negligible and detailed lineshape analyses were not required in the present context.

Since for H_2O and D_2O hydrated biomolecules the scattering is incoherent to a good approximation, the window-integrated (range $-2R < \hbar\omega < 2R$) elastic intensity, $S_{qe}(Q,T)$, is essentially proportional to a proton-weighted Debye–Waller factor in regions where the dynamic behavior is adequately described by a system of harmonic or quasi-harmonic oscillators. The average mean square proton mobility $\langle u^2\rangle$, can thus be derived from the slope of ln $S_{qe}(Q,T)$ *vs.* Q^2 for the three studied samples in the studied temperature range.

The inelastic part of the scattering spectra gives access to thermodynamic quantities *via* the vibrational density of states, $g(\omega)$ or VDOS, as they may be used to evaluate the heat capacity, C_p, for comparison with the obtained calorimetric data. Therefore the vibrational density of states (VDOS) were extracted from the obtained spectra and the corresponding heat capacity values obtained according to the formalism described below.[60]

The value for $g_i(2\theta,\omega) = I(2\theta,\omega) \times \omega$/Bose population factor $(\omega,T_{sample})/Q(2\theta,\omega)^2$ is calculated for each angle, where $I(2\theta,\omega)$ is the intensity detected with an energy exchanged of ω on a detector oriented at 2θ and the Bose population factor is $[\exp(\hbar\omega/kT) - 1]^{-1}$. The vibrational density of states then writes:

$$g(\omega) = \int_0^\infty g_i(\theta,\omega)\mathrm{d}\theta$$

According to Klug *et al.*[61] the vibrational heat capacity can be accurately estimated below 100 K from the inelastic neutron spectra (INS) using the harmonic oscillator model

$$C_v = R\int_0^\infty \frac{g(\omega)(\hbar\omega/kT)^2\exp(\hbar\omega/kT)}{[\exp(\hbar\omega/kT) - 1]^2}\mathrm{d}\omega$$

where C_v is the isochoric molar heat capacity, R is the gas constant, $\hbar$ is Planck's constant, ω is the phonon frequency, k is Boltzmann's constant and $g(\omega)$ is the vibrational density of states (VDOS).

The anharmonic part of the specific heat associated with the thermal expansion $C_p - C_v = TV\alpha^2/\kappa_T$ (where V is the molecular volume, α is the volume thermal expansion, and κ_T is the isothermal compressibility) is estimated to be negligible (0.025 J mol^{-1} K^{-1}) at 100 K,[62] and thus the isobaric heat C_p capacity is virtually indistinguishable from the isochoric specific heat C_v. Above 100 K, the vibrational heat capacity of ice becomes noticeably anharmonic[61] and deviations of calculated heat capacity from the experimental values are expected.

The theory is exact for simple crystals and valid to a good approximation for amorphous systems with dominant incoherent scattering. In biomolecules, on average, every second atom is a proton and their roughly homogeneous distribution reflects the collective dynamics. Also as the neutron proton is a nuclear interaction, no selection rule applies, so that $g(\omega)$ can be considered as a genuine VDOS. The $\hbar\omega$ region over which this is reasonable depends on various factors (residual contribution of coherent scattering, Q-range, degree of multi-phonon scattering) but in general extends to 40–50 meV. For fundamental reasons, specific heats derived from $g(\omega;T)$ (*via* multiplication by the quantal heat capacity per mode and ω-integration) cannot be expected to be equal to thermodynamically determined C_p values, but the T-dependence should be nearly the same and should sensitively reflect changes in the proton *vs.* heavy atom energetics.

2.4. Adiabatic calorimetry experiments

Heat capacity measurements were carried out in a laboratory-made adiabatic calorimeter for small samples[63] in the temperature region of 5–300 K. The sample masses used for the measurements were 0.77388, 0.20879, 0.15958, and 0.14881 g for the samples with h = 4.51, 0.49, 0.14, and 0.060 (mass of water/mass of peptide), respectively. Buoyancy correction was made to all the sample masses. Each sample was set into a 1.1 cm^3 gold-plated copper cell and sealed with an indium wire in atmospheric helium gas to promote thermal equilibration in the cell. Thermometry was performed with a rhodium-iron alloy resistance thermometer (nominal 27 Ω, Oxford Instruments) calibrated on the basis of the international temperature scale of 1990 (ITS-90).

The samples were cooled down at a rate of *ca.* 1 K min^{-1}, and then the heat capacities were measured at a rate of *ca.* 0.1 K min^{-1}. This was not done by continuous heating but by discontinuous, stepwise heating.

3. Results

3.1. Neutron scattering

The quality of the spectra obtained at LLB with MIBEMOL for the long runs is such that small INS differences down to a few 10^{-4} of $S(Q,0)$ are analyzable with confidence. By contrast, individual spectra from the continuous T-scan with the same instrument are statistically poor in the IE region proper, but their window-integrated quasi-elastic intensities provide $S_{qe}(Q,T)$ functions over a T-grid with statistics good enough to detect the temperature where the dynamics begins to be affected by softer modes and anharmonic interactions.

The obtained values of $\langle u^2\rangle$ as a function of temperature for the D_2O, nominally dry and H_2O hydrated samples can be seen in Fig. 1 and 2.

The D_2O hydrated sample shows three regions in the temperature dependence of $\langle u^2\rangle$ values; (i) at $T < \sim 150$ K a linear increase with temperature is observed; (ii) between 150 and 220–230 K the values increase with a higher slope; and finally (iii) above 220–230 K there is an even steeper increase in $\langle u^2\rangle$ with temperature. As we are dealing with a sample hydrated with heavy water, the increase in slope in the intermediate region reflects protein dynamics. Further, our small peptide is likely to have significant hydration-induced side chain mobility at low temperatures. The steeper increase above 220–230 K is

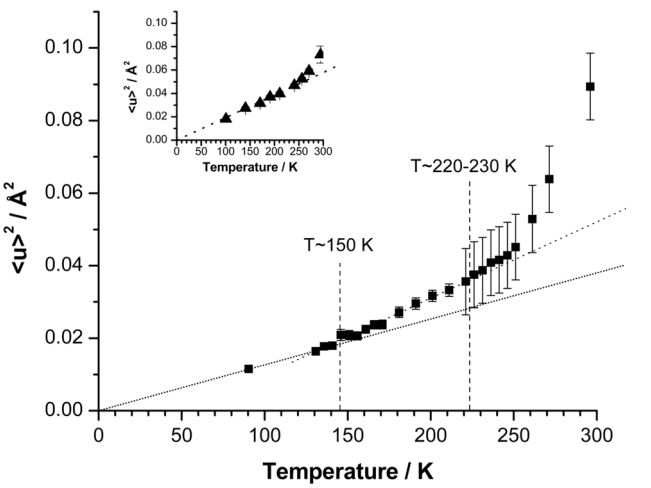

Fig. 1 Proton mobility $\langle u^2\rangle$, as a function of temperature for the D_2O hydrated sample (h = 0.51). The dotted line represents the low- and intermediate-temperature behavior, and the dashed vertical lines the approximate locus arround which a change in temperature trend is apparent. The error bars are twice the error obtained from the calculation. Inset: proton mobility $\langle u^2\rangle$ as a function of temperature for the nominally dry sample (h = 0.060, sample with residual H_2O).

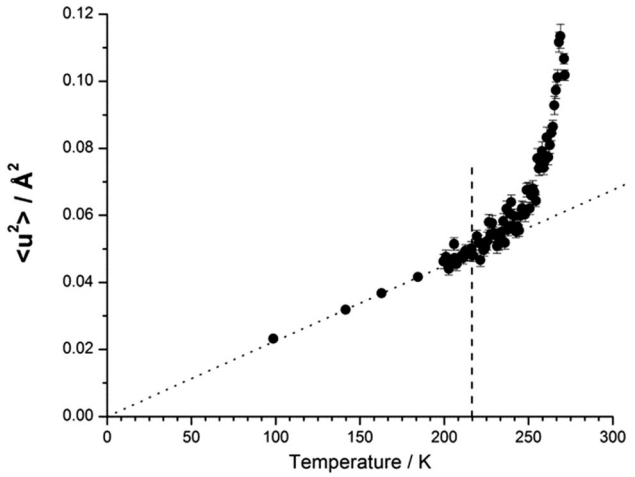

Fig. 2 Proton mobility $\langle u^2 \rangle$, as a function of temperature for the H_2O hydrated sample (h = 0.49). The dotted line represents the low-temperature behavior, and the dashed line the approximate locus arround which a change in temperature trend is apparent. The error bars are twice the error obtained from the calculation.

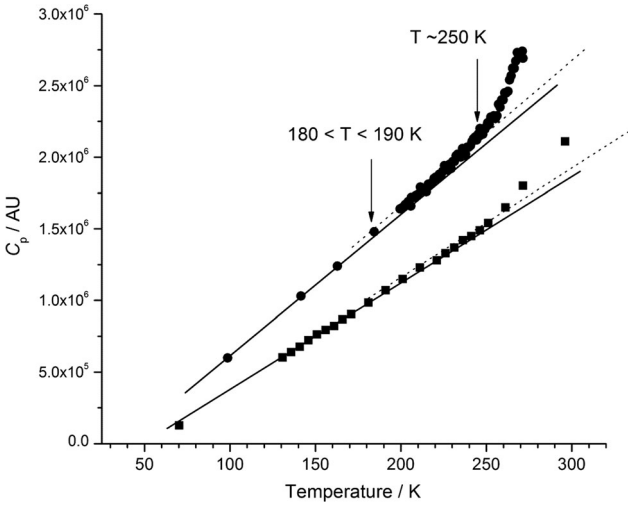

Fig. 3 Plot of C_p values as obtained from VDOS as a function of temperature for the H_2O (h = 0.49) and D_2O (h = 0.51) hydrated samples. The lines represent the observed trends and are just a ''guide for the eye''.

usually correlated with the so called dynamic transition, reflecting the increase in internal rotation and translation dynamics.[9,12,13,23,24,28,32] The $\langle u^2 \rangle$ values for a nominally dry sample (Fig. 1, inset) shows linear temperature dependence up to about 240 K, and a deviation from linearity above this temperature. Nevertheless, a plot of the summed elastic intensity *vs.* temperature indicates the possibility of a change in the slope of the temperature dependence around 150 K (results now shown). We should remember that we called it ''nominally dry'' because the usually called dry protein samples always have some structural water. In our case, we know that our sample has h = 0.060 (g H_2O/g CA(1–7)M(2–9)). Thus, this water can provide the necessary plasticity for peptide chain movements to be facilitated at low temperature.

In the case of the H_2O hydrated sample, we are observing a mixture of protein and water dynamics (Fig. 2). Despite the dispersion of the data in the intermediate temperature range (data from elastic scan, with poorer statistics), we can clearly see a steeper increase in $\langle u^2 \rangle$ above 220–230 K. The low temperature break around 150 K that was clearly observed for the D_2O hydrated sample cannot be detected here because we did not cover this temperature region so extensively for the H_2O hydrated sample, as we already had the protein dynamics information in this range from the deuterated sample.

The values of heat capacity as obtained from the VDOS for the H_2O and D_2O hydrated samples can be seen in Fig. 3, plotted as a function of temperature. The values are in arbitrary units, and normalized to the total mass (peptide + H_2O or D_2O) of respective samples. The obtained C_p values for both samples clearly show 3 temperature dependence regimes – a linear trend for the low temperatures, followed by a jump to higher values at about 185 K, keeping the growth at about the same pace up to about 250 K, and finally a steeper increase for T > 250 K. Indeed the values for the H_2O hydrated sample are higher, due to the larger incoherent contribution (see Table 2), but the same trend as a function of temperature is apparent in both samples.

3.2. Adiabatic calorimetry

3.2.1. Heat capacity. Heat capacities C_p (per mole of CA(1–7)M(2–9)) and spontaneous temperature drift rates of all the samples are plotted against temperature T in Fig. 4 and 5, respectively. All samples were first cooled from room temperature to 6 K at a rate of *ca.* 1 K min^{-1}. We designate these samples as ''normally cooled'' samples. The normally cooled samples with water contents h = 4.51 and 0.49 exhibited broad heat capacity jumps at temperatures below 200 K, where changes from exothermic to endothermic temperature drift rates were observed. This behavior is characteristic of a glass transition.[64] Between 200 and 250 K, the temperature of the samples kept under adiabatic conditions increased spontaneously during the measurements. This exothermic effect is caused by crystallization of part of the water present in the samples. Further, fusion of ice was observed at temperatures T_{fus} = 272.5 and 265.0 K for the h = 4.51 and 0.49 samples, respectively (Fig. 4 and 5).

These samples were next kept under adiabatic conditions, *i.e.*, ''annealed'' around 230 K for about one day until the spontaneous exothermic effect disappeared. The results for the annealed samples are also shown in Fig. 4 and 5. Similar but less pronounced glass transitions were found around the same temperatures as the ones observed in the normally cooled samples.

The normally cooled sample with h = 0.14 also presents a broad glass transition around 220 K, but it did not show the exothermic effect that was observed in the samples with higher hydration levels, which we assigned to crystallization of water and fusion of ice. The nominally dry sample (h = 0.060) did not show any of these thermal events in the present temperature range (and within the instrument sensitivity).

3.2.2. Fusion of water. The enthalpies of fusion of water in the hydrated annealed samples were calculated as explained below, and expressed per mole of CA(1–7)M(2–9).

Table 2 Experimental enthalpy of fusion of hydration water (expressed per mole of CA(1–7)M(2–9), here stated as CM15) and calculated amounts of ''free'' (frozen) and ''bound'' (unfrozen) water (also expressed per mole of CA(1–7)M(2–9), CM15) as explained in the text for each peptide sample at different water contents, h

h	$\frac{10^{-3}\Delta_{fus}H}{\text{kJ mol}_{CA(1-7)M(2-9)}^{-1}}$	$\frac{n_{H_2O}(\text{frozen})}{\text{mol}_{CA(1-7)M(2-9)}}$	$\frac{n_{H_2O}(\text{unfrozen})}{\text{mol}_{CA(1-7)M(2-9)}}$	$\frac{n_{H_2O}(\text{total})}{\text{mol}_{CA(1-7)M(2-9)}}$
4.51	2.498	416.0	27.7	443.7
0.49	0.1332	22.2	25.7	47.9
0.14	0	0	13.7	13.7
0.060	0	0	6.0	6.0

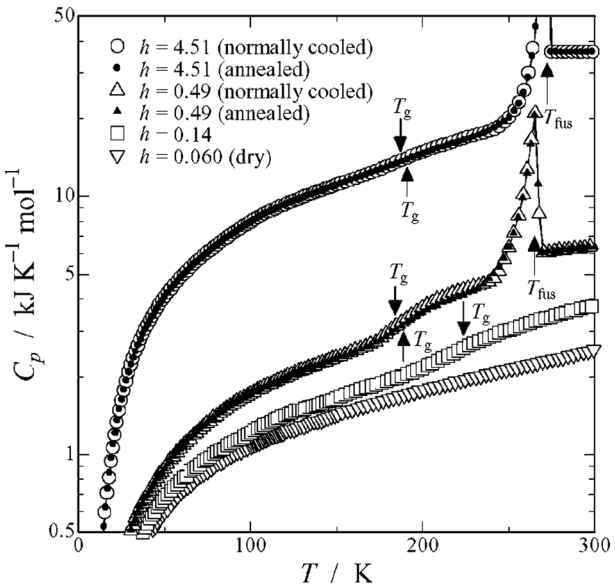

Fig. 4 Heat capacities (C_p) per mole of CA(1–7)M(2–9) of samples with h = 4.51, 0.49, 0.14, and 0.060 as determined by adiabatic calorimetry.

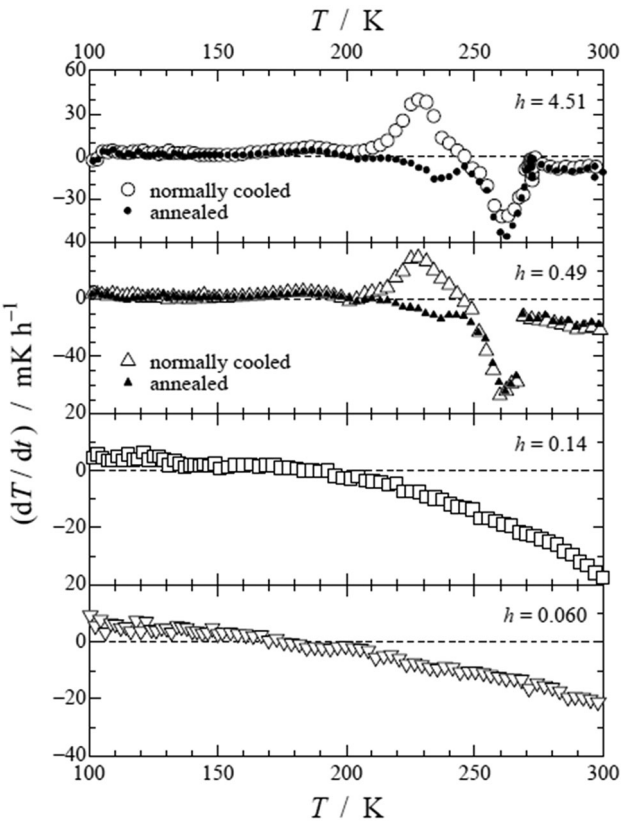

Fig. 5 Temperature drift rates of samples with hydration values h = 4.51, 0.49, 0.14, and 0.060.

For the sample with h = 4.51, a straight line and a second-order curve were fitted to the C_p data between 214 and 227 K and between 274 and 302 K, respectively. For the sample with h = 0.49, two straight lines were fitted to the C_p data between 214 and 221 K and between 270 and 300 K, respectively. The baseline heat capacities were determined by extrapolating the lower fitted function up to and the upper fitted function down to the melting points of ice (272.5 and 265.0 K, respectively, for each of the samples). The enthalpies of fusion were calculated by subtracting the contribution of the base line heat capacity from the total enthalpy change.

From the evaluated experimental enthalpies of fusion, the amount of frozen water was estimated by use of the literature enthalpy of fusion of pure water at 0 °C,[65] $\Delta_{fus}H$ = 6.0068 kJ mol^{-1}, assuming that this water is ''free water'' and therefore the energy involved in fusion can be calculated from the enthalpy of fusion of pure water. The amount of unfrozen water was thereafter obtained by subtracting the amount of frozen water from the total water present in the sample. The enthalpies of fusion of hydration water (expressed per mole of CA(1–7)M(2–9)) are presented in Table 2 for the sample with hydrations h = 4.51 and 0.49 together with the number of moles of frozen and unfrozen water per mole of peptide for all hydrated samples.

These results reveal that there are at least two types of water in the hydrated samples: freezable water (free water) and unfreezable water (bound water). Further, based on our results we can also say that in the h = 4.51 and 0.49 samples there are two kinds of free water: rapidly freezable water and slowly freezable water, as inferred from the appearance of an exothermic effect which we assigned to freezing of a part of the hydration water in the normally cooled samples above the glass transition temperature. This effect may be called ''annealing-induced'' crystallization, and will result in a smaller enthalpy of fusion for an experiment performed with a high heating rate.

In summary we can say that the peptide retains an amount of bound (unfreezable) water up to about 27 mol H_2O per mole of CA(1–7)M(2–9) (or about 0.25 g H_2O/g CA(1–7)M(2–9)). This value is in the lower end of the range of limiting hydration values commonly found for proteins, 0.3–0.5 g H_2O/g of protein.[66]

3.2.3. Glass transition. All hydrated samples (except the nominally nominally dry sample, h = 0.060) exhibited broad glass transitions. In order to examine this glassy behavior in more detail, the obtained heat capacities (C_p) were differentiated with respect to T by the moving-average method. The temperature derivatives of the heat capacities dC_p/dT for all studied samples are shown in Fig. 6.

Glass transition temperatures are more commonly determined as the temperature where an exothermic temperature drift turns to an endothermic one, because a heat capacity jump is observed around that temperature.[64] In the present work, however, we could not detect a glass transition temperature in this way because the change from exothermic temperature drift to endothermic one was smeared. In particular for the h = 0.14 sample, no temperature drift rate characteristic of a glass transition was observed (see Fig. 5). Therefore the glass transition temperatures were taken as the inflection points in C_p *vs.* temperature curves, *i.e.*, as the maxima of dC_p/dT around the glass transition region (as indicated in Fig. 6). The derived glass transition temperatures are 187 and 191 K for the normally cooled and annealed samples, respectively, with h = 4.51, 184 and 189 K for the normally cooled and annealed samples, respectively, with h = 0.49 and finally 224 K for the sample with h = 0.14.

As seen from Fig. 6, for the samples with h = 4.51 and 0.49 the magnitudes of the differential values dC_p/dT around the glass transition region are somewhat larger for the normally cooled samples than for the annealed ones. This reflects a larger increment of the heat capacity for the normally cooled samples as compared to the annealed ones in the glass transition region. The observed difference indicates that the glass transition is closely related to the water included in the samples – the normally cooled samples gave rise to crystallization of a part of their supercooled water at temperatures above the glass transition temperature and the C_p anomalies due to the glass transitions became smaller when a smaller fraction of the hydrated water was frozen on annealing.

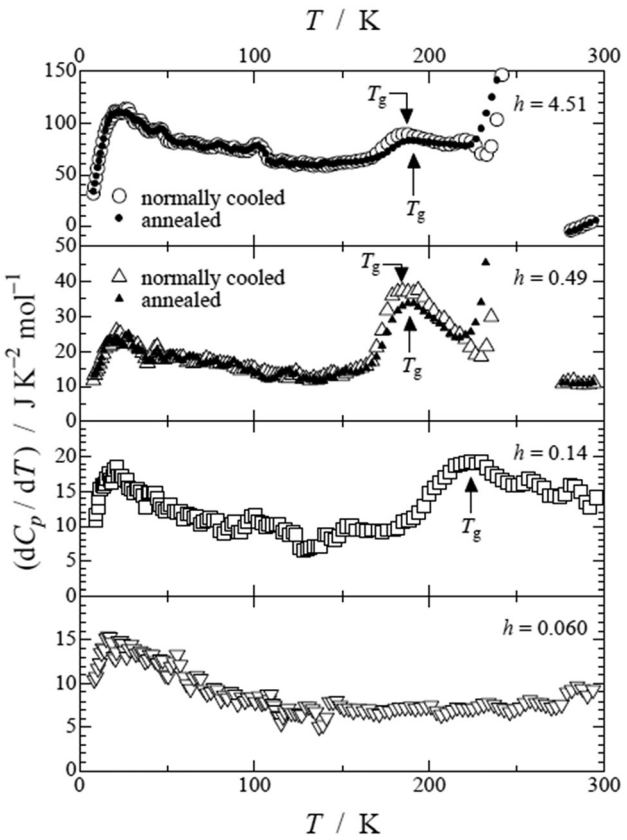

Fig. 6 Temperature derivatives of the heat capacity per mole of CA(1–7)M(2–9) for the samples with hydration values h = 4.51, 0.49, 0.14, and 0.060.

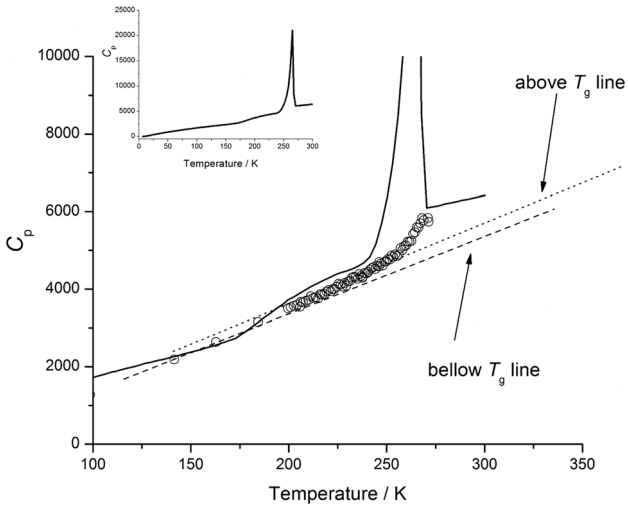

Fig. 7 Heat capacity values as derived from VDOS for the H_2O hydrated sample (appropriately scaled) (○) and as obtained from adiabatic calorimetry (full line) for the sample with h = 0.49 as a function of temperature. The plot covers the range of values (yy and xx) where the comparison can be made. The dotted and dashed lines represent the observed trends of the heat capacities derived from VDOS below and above T_g and are just a ''guide for the eye''. Inset: the full calorimetric C_p curve for the same sample (h = 0.49).

3.3. Comparison of the C_p values derived from adiabatic calorimetry and neutron scattering

The C_p values derived from the VDOS (Fig. 3) show a temperature dependence that is similar to those obtained from adiabatic calorimetry (Fig. 4) for the sample with a similar hydration level (h = 0.49). Therefore in order to enable a closer comparison, we did scale the neutron C_p values (in arbitrary units in Fig. 3) in order to allow a simultaneous plot with the calorimetric ones. The two sets of heat capacity data are plotted in Fig. 7 as a function of temperature.

4. Discussion

By calorimetry it is not possible to discriminate if the transitions observed are due to the protein, the hydration water or both. Therefore, a combined interpretation of results from the different techniques is needed for a full understanding of this problem. In the present work we did try to contribute to this effort by evaluating the mean-square displacements of samples of H_2O and D_2O hydrated peptides and extracting the vibrational

contribution to the heat capacity through calculation of C_p values from the VDOS derived from neutron scattering.

The change in slope of the temperature dependence of hydrated protein's mean-square displacement around 220 K has been extensively studied,[9,11,13,23,24,67,68] as this transition is connected to protein function and vanishes in the absence of hydration. It has been proposed that the dynamical crossover around 220 K could be associated with a large scale structural change in hydrogen bond connectivity.[13,28,49] Further, Zanotti *et al.*[13] propose that the water rotational dynamics of interfacial water is the real source of entropy-driven protein dynamics. A MD study by Tarek and Tobias,[19] on the other hand, suggests that translational motion of water is necessary for the structural relaxation that permits anharmonic and diffuse motion in proteins. Recent simulations of hydrated lysozyme showed accordingly that whereas hydration water has diffusive-like translational motion, proteins exhibit only localized atomic fluctuations on the pico- to nano-second time scale.[69] The same conclusions were drawn from a neutron scattering study of D_2O hydrated hydrogenated GFP (green fluorescent protein) and a H_2O hydrated sample of fully deuterated GFP.[9]

The values obtained for the proton mobility as a function of temperature for the two hydrated samples (Fig. 1 and 2) show three temperature dependence regions, in accordance with previous studies.[9,11,13] For the nominally dry peptide we did not observe a break in the temperature trend of $\langle u^2 \rangle$ values up to $\sim$240 K, as expected (Fig. 1, inset).

In the case of deuterium hydration, the increase in slope in the intermediate region reflects peptide dynamics. For proteins hydrated with heavy water, the increase in slope in the intermediate region has been assigned to the onset of methyl group rotation.[9] Russo *et al.*[70] refer to 50 K as the temperature of onset of methyl group dynamics and that two of their peptides (NALA and NAGMA) exhibit the same temperature dependence between 70 and 130 K, whereas NALMA shows a weaker temperature dependence, as a result of the presence of a hydrophobic side chain. In a study of lysozyme Roh *et al.*[11] observed the increase of a low-temperature anharmonicity around 100 K, irrespective of the hydration level. We should note that for our peptide 32% of non-exchangeable H-atoms are associated with CH_3 groups (5 of the 15 amino acid residues are lysine, and the peptide has 13 CH_3 groups), therefore this contribution must be significant. It is well known that methyl group dynamics varies widely, depending on conditions. We should stress that our peptide is a small peptide (15 aa), that is relatively unstructured under the conditions studied here. Thus the methyl group dynamics are expected to be faster, as compared to larger proteins.[9,11,33] Therefore, it cannot be ruled out that we can observe it within our timescale, with the instrument and conditions used. It can be argued, indeed, that they might not be observed in the same temperature range as in a globular protein. As we do observe the breaks as reported, we believe that it is the small size of the peptide and the absence of a marked secondary structure on the conditions used that allows us to see the methyl dynamics in approximately the same temperature range. Evidence for a continuity of relaxation processes in hydrated proteins has been provided by mechanical relaxation studies, shown to become active at temperatures as low as 155 K for lysozyme,[71] and they were regarded as a manifestation of glass-like relaxation behavior. These processes (secondary or β-relaxations) can be hard to detect by calorimetry, and are due to local rearrangements involving low energy barriers, such as methyl rotation in hydrated proteins or peptides. As for the higher temperature crossover, at temperatures above 220–230 K, it has been associated with large structural changes in hydrogen bond connectivity[13,28,33] and it is known that it does not show up in the absence of hydration. The departure of the mean square displacement of H-atoms, $\langle u^2 \rangle$, from their low temperature harmonic behavior at certain crossover temperatures cannot be straightforwardly related to the glass transitions, because of the different time scales of the processes – pico seconds as compared to usual relaxation times on the 100 s time scale. Nevertheless they may well be the triggering mechanism for the actual glass transition, enabling barrier-crossing processes involved in the molecular rearrangements that come into the experimental window at the calorimetric T_g.[72] The fact that we see this crossover temperature in both the H_2O and D_2O hydrated samples shows that protein dynamics are also enhanced in this temperature range. Yet the question remains whether these phenomena are connected. Zanotti *et al.*[13] stressed the importance of rotational dynamics of interfacial water as the real source of entropy driving protein dynamics, and thus concluded that the protein's external side-chain motion is induced by fast reorientational motion of water and that the two processes are strongly correlated. Trying to get further discrimination, the results of Nickels *et al.*[9] took advantage of the use of a D-protein that was H_2O hydrated and an H-protein that was D_2O hydrated. They report that no change in $\langle u^2 \rangle$ temperature dependence was observed up to 180–190 K for the H_2O hydrated d-GFP, showing that the dynamics of hydration water remains essentially harmonic up to these temperatures, whereas the D_2O hydrated h-GFP showed a clear change in slope already at $\sim$120 K, both in dry and hydrated states. Therefore, these authors conclude that the absence of anharmonic variation in the dynamics of hydration water up to 180 K indicates a complete decoupling of water and methyl group rotations. We would like to stress that we do not see these views as contradictory – in fact the results of Nickels *et al.*[9] led to the conclusion about the independence of water and methyl group rotations at low temperatures (below 180 K), whereas Zanotti *et al.*[13] provided evidence for the strong correlation between water dynamics and protein's slow, long range motion at temperatures above 220 K.

The results obtained from adiabatic calorimetry showed that the glass transition of hydrated CA(1–7)M(2–9) are related to the presence of water in the samples, as it is not observed in the dry sample (h = 0.060). However, the question arises as to whether the glass transitions should be attributed to the motion of the water molecules alone or to the combined effect of CA(1–7)M(2–9) and water molecules. According to the water content dependence of the glass transition temperature, we can see that the T_g is around 190 K for the samples with free water

(h = 4.51 and 0.49), while it increases to 224 K when the water content decreases and the sample has no free water (h = 0.14). Since the samples with h = 4.51 and 0.49 have a constant amount of bound water (*ca.* 27 mol H_2O/mol CA(1–7)M(2–9)), it follows that the glass transition temperature increases as the amount of the bound water decreases and does not seem to depend on the free water content. The recent work of Zhong *et al.*[15] also shows that there are two types of hydration water, those that reorient in the vicinity of a surface and those which are ordered, yet in dynamic interaction with the protein. Our results point in the same direction, as two types of water could be derived from the adiabatic calorimetry results and by neutron scattering we could see a strong correlation between water dynamics and protein's slow, long range motion at temperatures above 220 K, as discussed above. This latter effect can be explained as a plasticizing effect[73,74] in the sense that the hydration water can enhance protein flexibility. Consequently, the glass transitions in the hydrated CA(1–7)M(2–9) samples can be attributed to immobilization of the cooperative dynamics of the conformations of the CA(1–7)M(2–9) molecules and the bound water molecules.

The two hydrated samples (H_2O and D_2O) show harmonic behavior (*i.e.*, vibrational) up to about 160 K, and above this temperature the heat capacity values derived from VDOS increased above the values expected if only harmonic contributions were present (see Fig. 3). Around 180 K a shift to higher C_p values is observed, characteristic of a glass transition, occurring at a similar temperature to the T_g detected by adiabatic calorimetry (see Fig. 7) for the same hydration level (T_g = 184 and 189 K for the normally cooled and annealed samples, respectively, with h = 0.49). At ~240 K the VDOS heat capacity increased exponentially, in a region where by calorimetry we see the onset of fusion of water, for the sample with the same hydration level (onset of temperature increase due to crystallization is ~240 K and T_{fus} = 265.0 K for the sample with h = 0.49, Fig. 4 and 7). Again the two sets of results show agreement, as the onset of fusion of water should show as a huge increase in diffusive (translational/rotational) motion of the hydration water. Further, it is interesting to observe that after the phase transition (fusion) the VDOS derived heat capacities seem to level off to a position close to the retrieved baseline C_p as observed by calorimetry after fusion is completed.

Angell *et al.*[75] suggested that the continuous change in slope of the vibrational entropies mean that there is an almost discontinuous change in vibrational heat capacity due to the unfreezing of the structure, and that this change must be as abrupt as the change in total heat capacity observed in calorimetry at T_g. Further, in a sketch shown in the paper, the authors suggest that the vibrational contribution should be smaller than the total heat capacity. Our results show that we can indeed retrieve the change in heat capacity due to the glass transition from the C_p values obtained from VDOS, and further that the vibrational contribution is smaller than the total heat capacity as measured by adiabatic calorimetry, in full agreement with the previous suggestion. In the analysis of heat capacity and entropy changes in processes involving proteins Sturtevant[18] stated the importance of the vibrational contribution to these thermodynamic properties. He estimated the vibrational contribution to the unfolding ΔC_p of lysozyme at 273 K to be 8 or 10% of the total ΔC_p, depending on the value assumed for the change in conformational entropy at the same temperature. This result parallels the suggestion of Angell *et al.*[75] of the vibrational contribution being just a small part of the total observed heat capacity. The present results show that (i) the vibrational contribution to the heat capacity is a part of, and smaller than, the total heat capacity that can be measured for peptides (and proteins); and that (ii) we can retrieve the change in C_p at T_g from the vibrational heat capacity, in full agreement with previous suggestions by Sturtevant[18] and Angell *et al.*[75]

The fact that we can see a transition in the C_p values derived from VDOS for both the H_2O and D_2O hydrated samples at temperatures close to the glass transition (T_g) derived from calorimetry seem to indicate that both the protein and its hydration water have a vibrational contribution to this phenomenon, *i.e.*, the glass transition would result from the combined effect of the water dynamics (diffusive character) and the more localized protein dynamics. These two phenomena are most probably coupled in this temperature range, as discussed above in relation to $\langle u^2 \rangle$ behavior. Further, the glass-like transition is suppressed in our dry peptide sample (Fig. 4), as has also been reported for dry proteins,[11,26] indicating that the solvent molecules are involved with the activation of diffusive anharmonic motions.

5. Conclusion

The experiments discussed here represent an application of INS to an oligopeptide intermediate in size between small peptides and globular proteins. Our results demonstrate that neutron techniques can contribute valuable new information to peptide dynamics in a parameter domain that is not, or at least not easily, accessible by other techniques. Further, they show that the vibrational contribution to the heat capacity calculated from the INS data presents a temperature dependence similar to the one observed by adiabatic calorimetry, in particular allowing the detection of the glass transition in the same temperature range. Finally the results reiterate that both the peptide/protein and its hydration water (bound water) are involved in the crossover temperatures observed.

Acknowledgements

The experiments at LLB were supported by the European Commission through the Access Activities of the Integrated Infrastructure Initiative for Neutron Scattering and Muon Spectroscopy (NMI3), supported by the European Commission under the 6th Framework Program through the Key Action: Strengthening the European Research Area, Research Infrastructures, Contract no.: RII3-CT-2003-505925. Thanks are also due to Fundação para a Ciência e Tecnologia for financial support to CIQ(UP) through the strategic project Pest-C/QUI/UI0081/2011. MB would like to thank Patrick R. Connelly for

introducing her to Sturtevant's paper and the importance of vibrational contribution to the heat capacity of proteins.

References

1 M. Bastos, V. Castro, G. Mrevlishvili and J. Teixeira, *Biophys. J.*, 2004, **86**, 3822–3827.
2 M.-C. Bellissent-Funel, J. Teixeira, K. F. Bradley and S. H. Chen, *J. Phys. I*, 1992, **2**, 995–1001.
3 A. Cooper, *Biophys. Chem.*, 2005, **115**, 89–97.
4 A. Cooper, *J. Phys. Chem. Lett.*, 2010, **1**, 3298–3304.
5 F. Gabel and M.-C. Bellissent-Funel, *Biophys. J.*, 2007, **92**, 4054–4063.
6 I. Luque, S. A. Leavitt and E. Freire, *Annu. Rev. Biophys. Biomol. Struct.*, 2002, **31**, 235–256.
7 G. M. Mrevlishvili, A. P. S. M. C. Carvalho and M. A. V. Ribeiro da Silva, *Thermochim. Acta*, 2002, **394**, 73–82.
8 G. M. Mrevlishvili, A. P. S. M. C. Carvalho, M. A. V. Ribeiro da Silva, T. D. Mdzinarashvili, G. Z. Razmadze and T. O. Tarielashvili, *J. Therm. Anal. Calorim.*, 2001, **66**, 133–144.
9 J. D. Nickels, H. O Neill, L. Hong, M. Tyagi, G. Ehlers, K. L. Weiss, Q. Zhang, Z. Yi, E. Mamontov, J. C. Smith and A. P. Sokolov, *Biophys. J.*, 2012, **103**, 1566–1575.
10 P. L. Privalov and A. I. Dragan, *Biophys. Chem.*, 2007, **126**, 16–24.
11 J. H. Roh, J. E. Curtis, S. Azzam, V. N. Novikov, I. Peral, Z. Chowdhuri, R. B. Gregory and A. P. Sokolov, *Biophys. J.*, 2006, **91**, 2573–2588.
12 J. Teixeira, *Gen. Physiol. Biophys.*, 2009, **28**, 168–173.
13 J. M. Zanotti, G. Gibrat and M. C. Bellissent-Funel, *Phys. Chem. Chem. Phys.*, 2008, **10**, 4865–4870.
14 J.-M. Zanotti, M.-C. Bellissent-Funel and J. Parello, *Biophys. J.*, 1999, **76**, 2390–2411.
15 D. Zhong, S. K. Pal and A. H. Zewail, *Chem. Phys. Lett.*, 2011, **503**, 1–11.
16 H. D. Middendorf, N. Alves, J.-M. Zanotti, P. Gomes and M. Bastos, *Phys. B*, 2006, **385–386**, 874–876.
17 H. D. Middendorf, R. L. Hayward, S. F. Parker, J. Bradshaw and A. Miller, *Biophys. J.*, 1995, **69**, 660–673.
18 J. M. Sturtevant, *Proc. Natl. Acad. Sci. U. S. A.*, 1977, **74**, 2236–2240.
19 M. Tarek and D. J. Tobias, *Biophys. J.*, 2000, **79**, 3244–3257.
20 L. Foucat, J.-P. Renou, C. Tengroth, S. Janssen and H. D. Middendorf, *Appl. Phys. A: Solid Surf.*, 2002, **74**, S1290–S1292.
21 F. Gabel, D. Bicout, U. Lehnert, M. Tehei, M. Weik and G. Zaccai, *Q. Rev. Biophys.*, 2002, **35**, 327–367.
22 H. Jansson, R. Bergman and J. Swenson, *Phys. Rev. Lett.*, 2010, **104**, 017802.
23 K. Wood, A. Frolich, A. Paciaroni, M. Moulin, M. Hartlein, G. Zaccai, D. J. Tobias and M. Weik, *J. Am. Chem. Soc.*, 2008, **130**, 4586–4587.
24 K. Wood, M. Plazanet, F. Gabel, B. Kessler, D. Oesterhelt, D. J. Tobias, G. Zaccai and M. Weik, *Proc. Natl. Acad. Sci. U. S. A.*, 2007, **104**, 18049–18054.
25 S. Fujiwara, M. Plazanet, F. Matsumoto and T. Oda, *Biophys. J.*, 2008, **94**, 4880–4889.
26 H. Nakagawa, Y. Joti, A. Kitao and M. Kataoka, *Biophys. J.*, 2008, **95**, 2916–2923.
27 A. Orecchini, A. Paciaroni, A. D. Francesco, C. Petrillo and F. Sacchetti, *J. Am. Chem. Soc.*, 2009, **131**, 4664–4669.
28 J.-M. Zanotti, M.-C. Belissent-Funel and A. I. Kolesnikov, *Eur. Phys. J.: Spec. Top.*, 2007, **141**, 227–233.
29 H. D. Middendorf, *Nucl. Instrum. Methods Phys. Res., Sect. A*, 2009, **600**, 282–285.
30 M. T. F. Telling, C. Corsaro, U. N. Wanderlingh and H. D. Middendorf, *Chem. Phys.*, 2008, 245–249.
31 D. Russo, P. Baglioni, E. Peroni and J. Teixeira, *Chem. Phys.*, 2003, **292**, 235–245.
32 D. Russo, G. Hura and T. Head-Gordon, *Biophys. J.*, 2004, **86**, 1852–1862.
33 K. Wood, D. J. Tobias, B. Kessler, F. Gabel, D. Oesterhelt, F. A. A. Mulder, G. Zaccai and M. Weik, *J. Am. Chem. Soc.*, 2010, **132**, 4990–4991.
34 T. Hendrix, Y. V. Griko and P. L. Privalov, *Biophys. Chem.*, 2000, **84**, 27–34.
35 G. P. Privalov and P. L. Privalov, *Methods Enzymol.*, 2000, **323**, 31–62.
36 P. L. Privalov, *Crit. Rev. Biochem. Mol. Biol.*, 1990, **25**, 281–305.
37 X. Tadeo, M. Pons and O. Millet, *Biochemistry*, 2007, **46**, 917–923.
38 K. J. Breslauer, E. Freire and M. Straume, *Methods Enzymol.*, 1992, **211**, 533–567.
39 S. A. Leavitt, A. Schön, J. C. Klein, U. Manjappara, I. M. Chaiken and E. Freire, *Curr. Protein Pept. Sci.*, 2004, **5**, 1–8.
40 H. Ohtaka, S. Muzammil, A. Schon, A. Velazquez-Campoy, S. Vega and E. Freire, *Int. J. Biochem. Cell Biol.*, 2004, **36**, 1787–1799.
41 A. Velazquez-Campoy, S. Vega, E. Fleming, U. Bacha, Y. Sayed, H. W. Dirr and E. Freire, *AIDS Res. Rev.*, 2003, **5**, 165–171.
42 H. A. Filipe, F. M. Coreta-Gomes, A. Velazquez-Campoy, A. R. Almeida, A. F. Peixoto, M. M. Pereira, W. L. Vaz and M. J. Moreno, *J. Phys. Chem. B*, 2013, **117**, 3439–3448.
43 J. E. Ladbury, *Biochem. Soc. Trans.*, 2010, **38**, 888–893.
44 Y. Liu, A. Schon and E. Freire, *Chem. Biol. Drug Des.*, 2013, **81**, 72–78.
45 M. Sahun-Roncero, B. Rubio-Ruiz, G. Saladino, A. Conejo-Garcia, A. Espinosa, A. Velazquez-Campoy, F. L. Gervasio, A. Entrena and R. Hurtado-Guerrero, *Angew. Chem., Int. Ed.*, 2013, **52**, 4582–4586.
46 Y. Miyazaki, T. Matsuo and H. Suga, *Chem. Phys. Lett.*, 1993, **213**, 303–308.
47 Y. Miyazaki, T. Matsuo and H. Suga, *J. Phys. Chem. B*, 2000, **104**, 8044–8052.
48 G. M. Mrevlishvili, *Thermochim. Acta*, 1998, **308**, 49–54.
49 J.-M. Zanotti, M.-C. Belissent-Funel and S.-H. Chen, *Europhys. Lett.*, 2005, **71**, 91–97.
50 A. Lerbret, F. Affouard, P. Bordat, A. Hedoux, Y. Guinet and M. Descamps, *J. Chem. Phys.*, 2009, **131**, 245103.
51 D. Russo, J. Teixeira, L. Kneller, J. R. D. Copley, J. Ollivier, S. Perticaroli, E. Pellegrini and M. A. Gonzalez, *J. Am. Chem. Soc.*, 2011, **133**, 4882–4888.

52 H. Jansson and J. Swenson, *Biochim. Biophys. Acta*, 2010, **1804**, 20–26.
53 H. Boutin and S. Yip, *Molecular Spectrocopy with Neutrons*, MIT Press, Cambridge, MA, USA, 1968.
54 H. Boutin and W. L. Whittemore, *J. Chem. Phys.*, 1966, **44**, 3127–3128.
55 F. Abrunhosa, S. Faria, P. Gomes, I. Tomaz, J. C. Pessoa, D. Andreu and M. Bastos, *J. Phys. Chem. B*, 2005, **109**, 17311–17319.
56 M. Bastos, G. Bai, P. Gomes, D. Andreu, E. Goormaghtigh and M. Prieto, *Biophys. J.*, 2008, **94**, 2128–2141.
57 S. Trabulo, M. Mano, H. Faneca, A. L. Cardoso, S. Duarte, A. Henriques, A. Paiva, P. Gomes, S. Simoes and M. C. de Lima, *J. Gene Med.*, 2008, **10**, 1210–1222.
58 H. D. Middendorf and A. Miller, in *Neutrons in Biology*, ed. B. Schoenborn and R. Knott, Plenum Press, New York, 1996, pp. 239–265.
59 QENSH, http://www-llb.cea.fr/en/Phocea/Page/index.php?id = 21, accessed December 17, 2012.
60 A. A. Levchenko, A. I. Kolesnikov, N. L. Ross, J. Boerio-Goates, B. F. Woodfield, G. Li and A. Navrotsky, *J. Phys. Chem. A*, 2007, **111**, 12584–12588.
61 D. D. Klug, E. Whalley, E. C. Svensson, J. H. Root and V. F. Sears, *Phys. Rev. B: Condens. Matter Mater. Phys.*, 1991, **44**, 841–844.
62 G. P. Johari and O. Andersson, *Phys. Rev. B: Condens. Matter Mater. Phys.*, 2006, **73**, 094202.
63 Y. Kume, Y. Miyazaki, T. Matsuo and H. Suga, *J. Phys. Chem. Solids*, 1992, **53**, 1297–1304.
64 H. Suga and S. Seki, *J. Non-Cryst. Solids*, 1974, **16**, 171–194.
65 O. Haida, T. Matsuo, H. Suga and S. Seki, *J. Chem. Thermodyn.*, 1974, **6**, 815–825.
66 I. D. Kuntz Jr. and W. Kauzmann, *Adv. Protein Chem.*, 1974, **28**, 239–345.
67 W. Doster, *Eur. Biophys. J.*, 2008, **37**, 591–602.
68 M. Weik, U. Lehnert and G. Zaccai, *Biophys. J.*, 2005, **89**, 3639–3646.
69 L. Hong, N. Smolin, B. Lindner, A. P. Sokolov and J. C. Smith, *Phys. Rev. Lett.*, 2011, **107**, 148102.
70 D. Russo, M. A. Gonzalez, E. Pellegrini, J. Combet, J. Ollivier and J. Teixeira, *J. Phys. Chem. B*, 2013, **117**, 2829–2836.
71 A. V. Gorelov and V. N. Morozov, *Biophys. Chem.*, 1987, **28**, 199–205.
72 J. L. Green, J. Fan and C. A. Angell, *J. Phys. Chem.*, 1994, **98**, 13780–13790.
73 S. Bone and R. Pethig, *J. Mol. Biol.*, 1982, **157**, 571–575.
74 F. Parak, *Methods Enzymol.*, 1986, **127**, 196–206.
75 C. A. Angell, L. M. Wang, S. Mossa, Y. Yue and J. R. D. Copley, *AIP Conf. Proc.*, 2004, **708**, 473–482.